



Architecting Hierarchical WO₃ Agglomerates Assembled With Straight and Parallel Aligned Nanoribbons Enabling High Capacity and Robust Stability of Lithium Storage

Xiaotong Dong¹, Yongshuai Liu¹, Shikai Zhu¹, Yike Ou¹, Xiaoyu Zhang¹, Wenhao Lan¹, Haotian Guo², Cunliang Zhang^{2*}, Zhaoguo Liu¹, Shuai Ju¹, Yuan Miao¹, Yongcheng Zhang^{1*} and Hongsen Li^{1*}

OPEN ACCESS

Edited by:

Xifei Li,
Xi'an University of Technology, China

Reviewed by:

Ya You,
Wuhan University of Technology,
China
Xianhong Rui,
Guangdong University of Technology,
China

*Correspondence:

Hongsen Li
hsl@qdu.edu.cn
Yongcheng Zhang
qdzhy@163.com
Cunliang Zhang
zcliang@126.com

Specialty section:

This article was submitted to
Electrochemistry,
a section of the journal
Frontiers in Chemistry

Received: 13 December 2021

Accepted: 27 December 2021

Published: 02 February 2022

Citation:

Dong X, Liu Y, Zhu S, Ou Y, Zhang X,
Lan W, Guo H, Zhang C, Liu Z, Ju S,
Miao Y, Zhang Y and Li H (2022)
Architecting Hierarchical WO₃
Agglomerates Assembled With
Straight and Parallel Aligned
Nanoribbons Enabling High Capacity
and Robust Stability of
Lithium Storage.
Front. Chem. 9:834418.
doi: 10.3389/fchem.2021.834418

¹Center for Marine Observation and Communications, College of Physics, Qingdao University, Qingdao, China, ²School of Chemistry and Chemical Engineering, Henan Engineering Center of New Energy Battery Materials, Henan Key Laboratory of Bimolecular Reorganization and Sensing, Shangqiu Normal University, Shangqiu, China

The pursuit of electrochemical energy storage has led to a pressing need on materials with high capacities and energy densities; however, further progress is plagued by the restrictive capacity (372 mAh g⁻¹) of conventional graphite materials. Tungsten trioxide (WO₃)-based anodes feature high theoretical capacity (693 mAh g⁻¹), suitable potential, and affordable cost, arousing ever-increasing attention and intense efforts. Nonetheless, developing high-performance WO₃ electrodes that accommodate lithium ions remains a daunting challenge on account of sluggish kinetics characteristics and large volume strain. Herein, the well-designed hierarchical WO₃ agglomerates assembled with straight and parallel aligned nanoribbons are fabricated and evaluated as an anode of lithium-ion batteries (LIBs), which exhibits an ultra-high capacity and excellent rate capability. At a current density of 1,000 mA g⁻¹, a reversible capacity as high as 522.7 mAh g⁻¹ can be maintained after 800 cycles, corresponding to a high capacity retention of ~80%, demonstrating an exceptional long-durability cyclic performance. Furthermore, the mechanistic studies on the lithium storage processes of WO₃ are probed, providing a foundation for further optimizations and rational designs. These results indicate that the well-designed hierarchical WO₃ agglomerates display great potential for applications in the field of high-performance LIBs.

Keywords: WO₃, hierarchical structure, nanoribbons, lithium-ion batteries, high performances

INTRODUCTION

The commercialization of electrochemical energy storage (EES) systems, especially lithium-ion batteries (LIBs), has brought revolutionary changes in the industrial structure of energy storage (Abakumov et al., 2020; Liu L. et al., 2020; Eum et al., 2020; Gao et al., 2020). However, in spite of the mature technology of LIBs, which undergoes uncasting optimization for decades, the LIB systems are still seriously bottlenecked by conventional graphite materials on account of their low theoretical

capacities, thus severely restricting the overall energy density of EES devices (Zhang and Qi, 2016; Qu et al., 2019). In this respect, considerable efforts were devoted to design and exploit novel alternative anode materials with larger reversible capacity and energy density (Li H. et al., 2021; Li Q. et al., 2021; Yue et al., 2022). As a renowned part of the potential electrode material family, tungsten trioxide (WO₃) has attracted tremendous attention due to its excellent chemical stability, high theoretical capacity (693 mAh g⁻¹), and low cost (Yao et al., 2017; Bekarevich et al., 2020).

Although WO₃ has been widely investigated as hosts for energy storage, the applications of WO₃ in LIBs are still hindered by its intrinsic inferior conductivity and large volume strain, resulting in poor rate capabilities, sluggish kinetics, and rapid capacity fading in practical applications, thus seriously inhibiting its further development (Sasidharan et al., 2012; Yoon et al., 2014; Bekarevich et al., 2020; Xiao Y. et al., 2021; Rastgoo-Deylami et al., 2021; Hou et al., 2022). To conquer the obstacles above, various strategies have been approached in recent reports, in which the well-known examples of one-dimension (1D) structure offered the natural starting point (Luo et al., 2021). 1D single crystal WO₃ nanowires fabricated by Gu et al. delivered a discharge capacity of 218 mAh g⁻¹ for the first cycle under a current of 50 mA g⁻¹, and a capacity retention of 75.2% after 50 cycles, which can be largely attributed to the robust structural stability given by the 1D structure (Gu et al., 2007; Huang et al., 2020; Li et al., 2020). On the other hand, hierarchical structures have demonstrated their favorable Li-ion storage properties (Zhao et al., 2019; Liang et al., 2022). Duan et al. prepared biconical hexagonal (h-WO₃) mesocrystals by an ionic liquid-assisted hydrothermal route; the specific capacity of h-WO₃ mesocrystals can be maintained at 426 mAh g⁻¹ at 50 mA g⁻¹ after 50 cycles, benefiting from its inherent uniform porosity associated with well-defined nanoparticle orientation (Duan et al., 2015; Liu C. et al., 2020). However, noticeable capacity degradation was observed (1,379 mAh g⁻¹ for initial discharge and 30.9% capacity retention on 50th cycle). Beyond these, vacancy engineering (Tu et al., 2018; Li et al., 2019) or developing hybridization of WO₃ with conductive carbon-based materials (Yu et al., 2013; Di et al., 2019; Lee et al., 2021) have also been used to lower the bandgap and diffusion barriers, but the capacity retention is still limited during prolonged cycling. In this respect, despite these attempts, it remains an enormous challenge to improve the specific capacity and cyclic stability concurrently to satisfy future large-scale commercial applications (Xiao Z. et al., 2021; Du et al., 2021).

In light of the above consideration, herein, the well-designed WO₃ agglomerates assembled with straight and parallel aligned nanoribbons are prepared *via* a one-step hydrothermal method for high-performance LIBs. Benefiting from the unique hierarchical structure of WO₃ agglomerates with high electrode-electrolyte contact area, short Li-ion pathway, and good strain accommodation, the electrode exhibits dramatically enhanced Li-ion storage properties in cyclic

stability, specific capacity concurrently, along with a high capacity retention of ~80% (661.5 mAh g⁻¹ for initial discharge and 522.7 mAh g⁻¹ after 800 cycles at 1,000 mA g⁻¹), remarkably higher than those of the state-of-the-art WO₃-based anodes. Moreover, kinetics analysis and Li-ion diffusion chemistry of the hierarchical WO₃ agglomerates are investigated, providing a deeper insight into the mechanical origins of the improvement on Li-ion storage properties. These intriguing findings showcase the intrinsic desirable Li-ion storage performance of the hierarchical WO₃ agglomerates and open new opportunities for the applications of high-performance LIBs by informing more rational designs.

EXPERIMENTAL SECTION

Synthesis of Hierarchical WO₃ Agglomerates

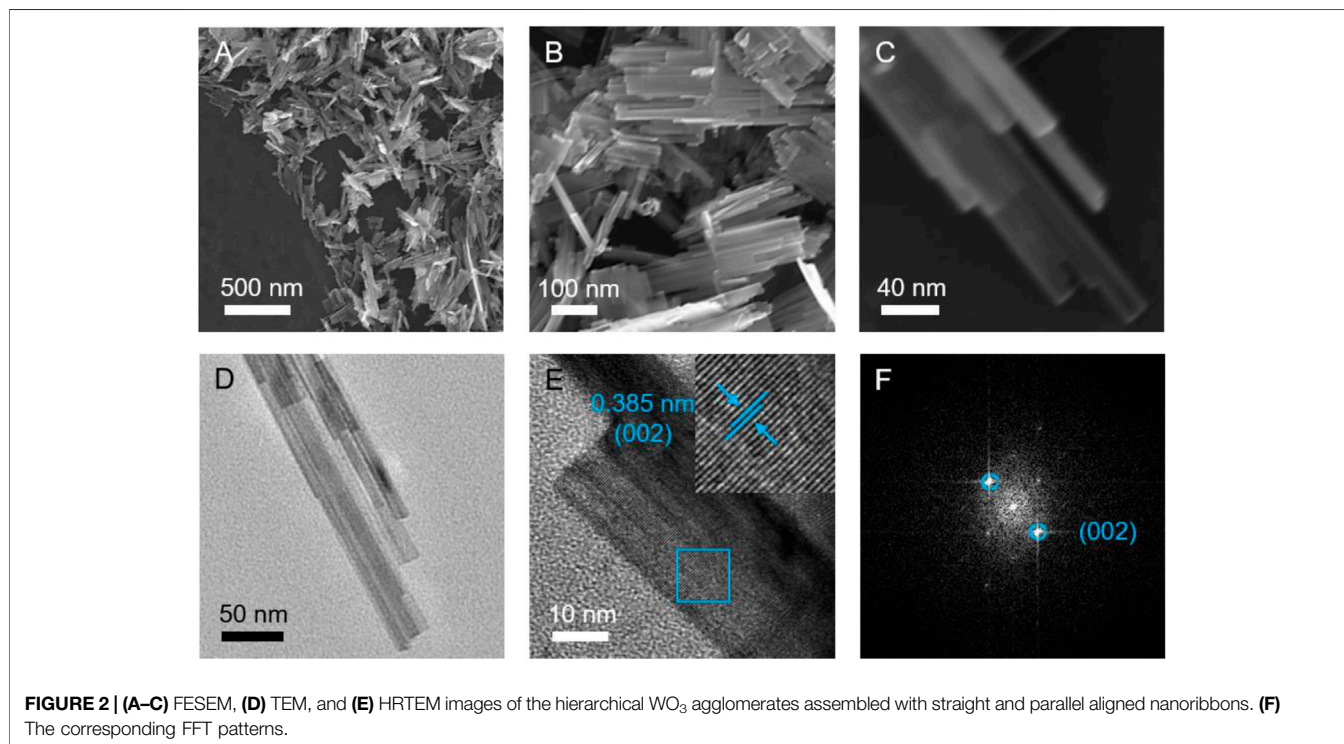
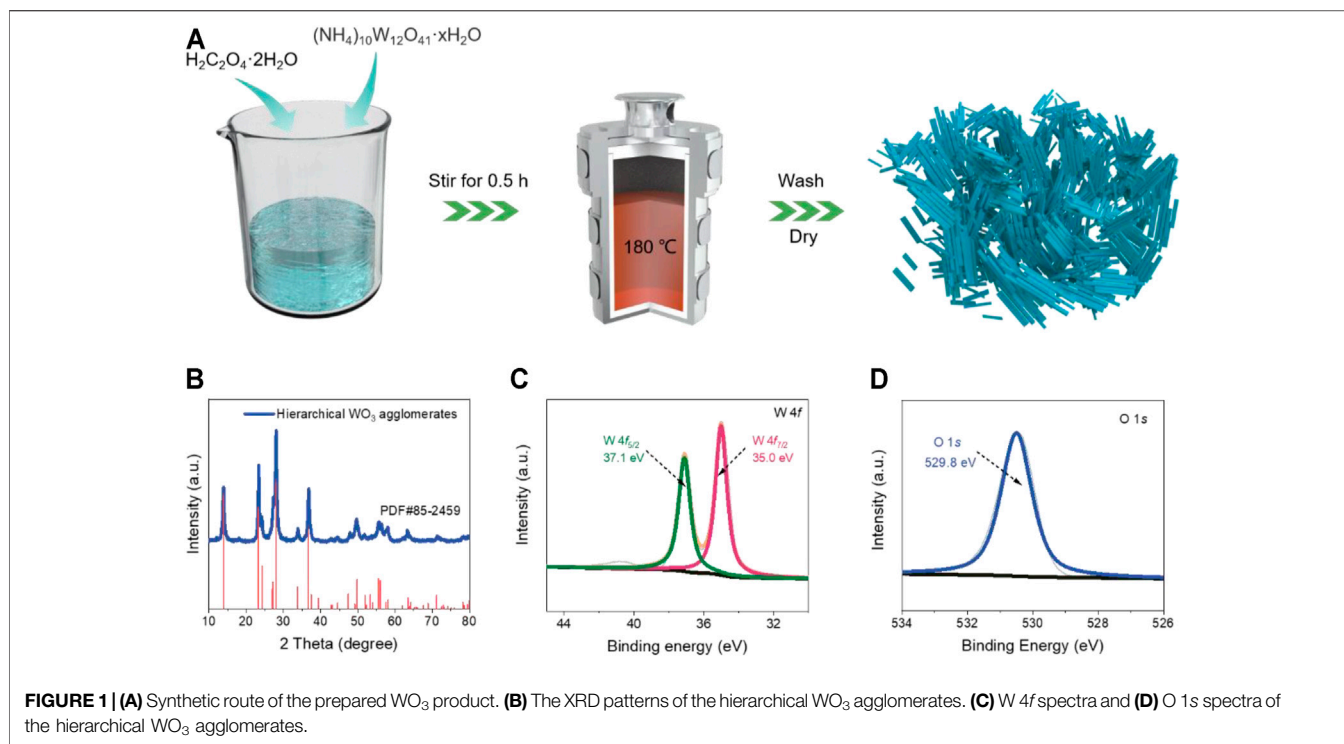
All the chemicals were used as received without further purifications. In a typical synthesis of hierarchical WO₃ agglomerates, 0.3 g of (NH₄)₁₀W₁₂O₄₁·xH₂O and 0.2 g of C₂H₂O₄·2H₂O dispersed in 30 ml of deionized water. After stirring for 30 min, the homogeneous solution was transferred into a 60-ml Teflon-lined autoclave and hydrothermal reaction proceeded at 180°C for 8 h in an electric oven. After cooling to room temperature, the obtained products were washed sequentially with deionized water and ethanol for three times, and they were finally dried overnight at 60°C. For comparison, pure WO₃ with different morphologies were synthesized *via* the same route except that the hydrothermal time was set as 4 and 12 h, respectively.

Material Characterization

The phase purity of the products was detected by powder X-ray diffraction (XRD, Bruker D8 Advance, Germany) with a Cu K α radiation. X-ray photoelectron spectroscopy (XPS) measurements were performed by an ESCALAB250Xi system using a monochromatic Al K α 1 source. The surface morphology of materials was explored by field-emission scanning electron microscopy (FESEM, ZEISS, Sigma-300) and transmission electron microscopy (TEM, JEOL, JEM-2100F).

Electrochemical Measurement

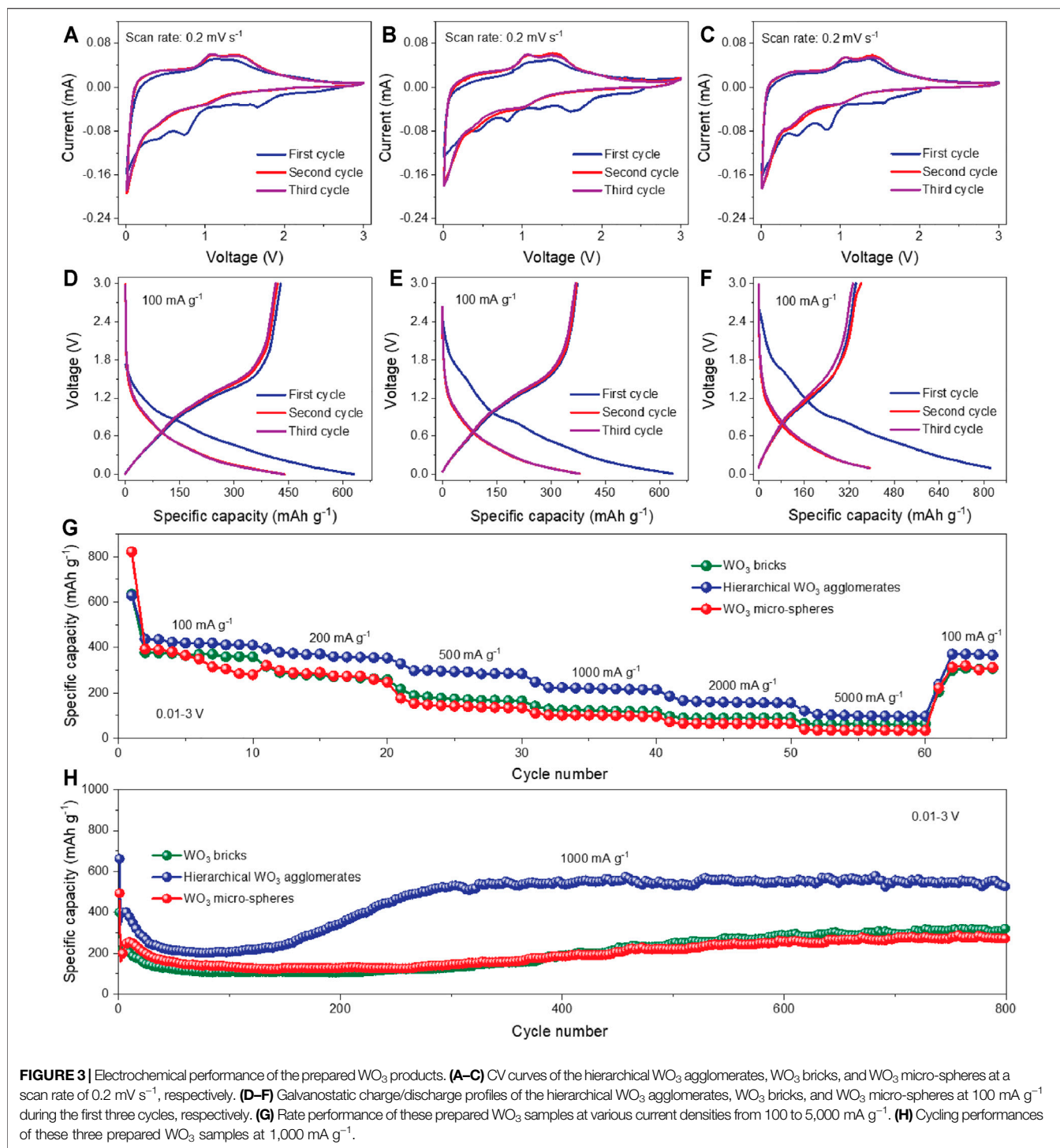
The working electrode slurries were obtained by mixing the active materials, Super P, and carboxyl methyl cellulose (CMC) (weight ratio = 7:2:1) in deionized water. The obtained slurries were coated on the copper foil; 1 M solution of LiPF₆ in ethylene carbonate (EC)/dimethyl carbonate (DMC)/diethyl carbonate (DEC) with a volume ratio of 1:1:1 was employed as the electrolyte, and the Celgard 2,250 film (Whatman) was selected as separator. The galvanostatic discharge-charge measurements were performed on a multichannel battery tester (LAND-CT2001A). The cyclic voltammetry (CV) and electrochemical impedance spectroscopic (EIS) curves were conducted on an electrochemical workstation (IVIUM technologies, Vertex).



RESULTS AND DISCUSSION

Figure 1A provides a schematic description of the synthesis strategy of the hierarchical WO₃ agglomerates, which was

prepared *via* a simple one-step hydrothermal method using (NH₄)₁₀W₁₂O₄₁·xH₂O as the tungsten source (details are described in the Experimental section). Through regulating the hydrothermal time, the pure WO₃ products with controllable



morphology could be obtained. The XRD testing was first carried out to investigate the phase purity of the as-prepared products. As shown in **Figure 1B**, the green lines stand for the final products. The obvious sharp and strong diffraction peaks indicates high-crystallinity of WO₃, which can be well indexed to typical hexagonal (JCPDS No. 85-2459) phase without any unknown impurity peaks (Pachfule et al., 2016). The XPS spectrum was also

performed to analyze the elemental composition and surface chemical bonding state of the products (Tong et al., 2016). The survey spectrum shows that the prepared WO₃ consists of C, O, and W elements (**Supplementary Figure S1**). The high-resolution XPS of W 4f (**Figure 1C**) exhibits two characteristic peaks located at 35.0 and 37.1 eV that correspond to the W 4f_{7/2} and W 4f_{5/2} levels (Grugeon et al., 2001). The O 1s XPS spectra in

Figure 1D shows the peaks at 529.8 eV, which is ascribed to the W-O bonding mode of WO₃ (Poizot et al., 2000). The XPS results further confirm the phase purity of WO₃, in keeping with the above XRD analysis.

To study the morphologies and microstructures of the prepared WO₃ products, FESEM and TEM were conducted (**Figure 2**). As displayed in **Figures 2A–C**, the structure of product consists of straight and parallel aligned nanoribbons with a periodic stacking. These secondary 1D nanoribbons have a diameter of approximately 20 nm, offering abundant active sites for lithium ions/electrons exchange between the electrode and the electrolyte, (Liu L. et al., 2020), which is conducive to achieving good electrochemical performances. **Supplementary Figure S2** and **Supplementary Figure S3** exhibit the FESEM images of the contrast samples synthesized under different hydrothermal time. Interestingly, with the decrease of the hydrothermal time, the product features a multilayer brick morphology (**Supplementary Figure S2**, denoted as WO₃ bricks); however, when the hydrothermal time increases, a micro-sphere assembled with some irregular nanoribbons can be obtained (**Supplementary Figure S3**, denoted as WO₃ micro-spheres). It can be seen that the hydrothermal time plays a key role in the formation of the different structures of the WO₃ electrode. In addition, the XRD patterns of the above-mentioned WO₃ bricks and WO₃ micro-spheres were also tested, which can be found in **Supplementary Figure S4** and **Supplementary Figure S5**, respectively. TEM and high-resolution TEM (HRTEM) images of the hierarchical WO₃ agglomerates (shown in **Figures 2D,E**) further reveal the crystallographic orientation and unique stacking straight and parallel aligned nanoribbons structure (Chen et al., 2019). The lattice-resolved HRTEM image exhibits the clear lattice with a spacing of 0.385 nm for the (002) planes of WO₃ (**Figure 2E**). Moreover, the corresponding fast Fourier transform (FFT) pattern (**Figure 2F**) also shows the existence of (002) facets, further confirming the high purity of the prepared WO₃.

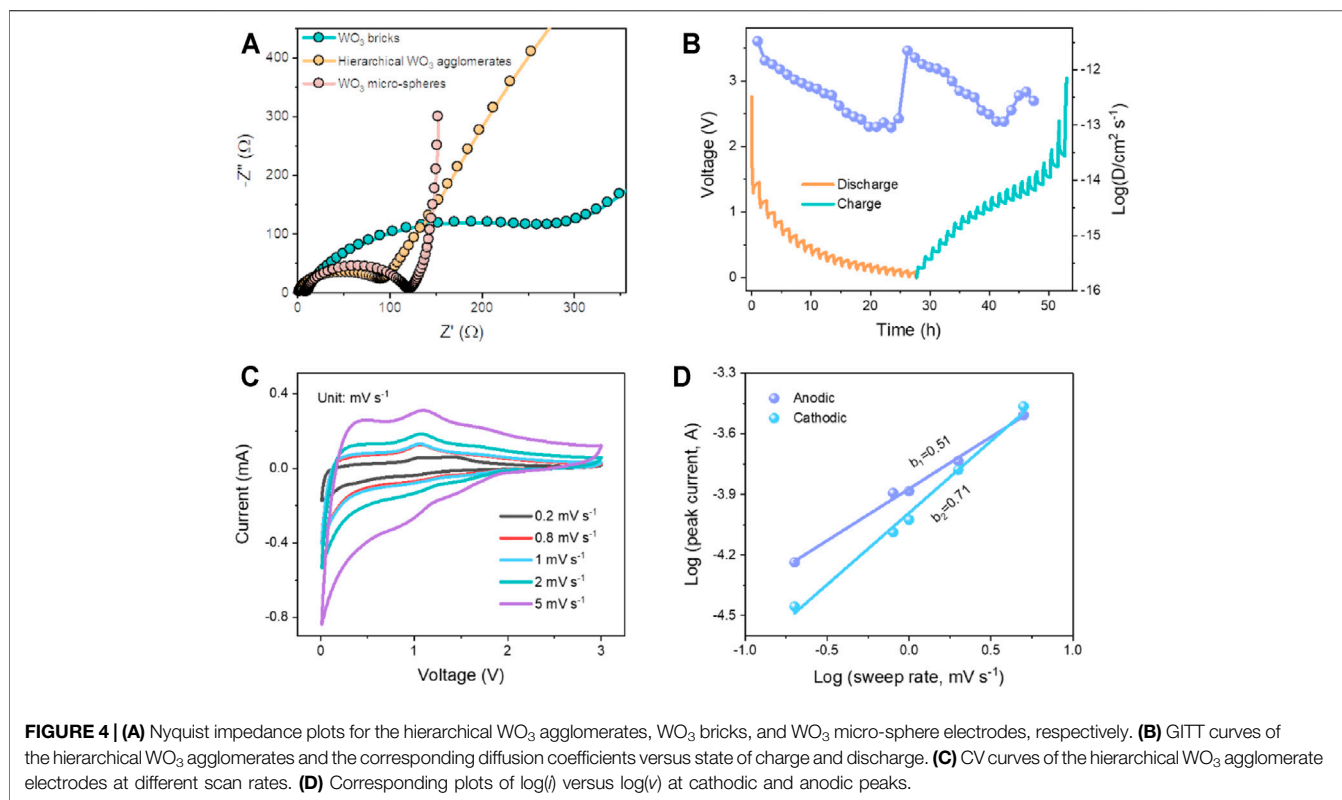
To explore the potential of these as-prepared WO₃ products for Li-ion storage, half-cells were assembled with Li metal as the counter and reference electrodes. The CV curves of the hierarchical WO₃ agglomerates at a scan rate of 0.2 mV s⁻¹ in the voltage window of 0.01–3.0 V (vs. Li/Li⁺) are presented in **Figure 3A**. Apparently, the reduction peaks between 0.3 and 2 V in the cathodic polarization process are observed in the first cycle, which can be ascribed to the decomposition of the electrolyte and the formation of the solid–electrolyte interface (SEI) (Dahbi et al., 2016; Wang et al., 2018; Yao et al., 2018; Huang et al., 2020). On the following cycles, the broad reduction peak at ~1.0 V on the cathodic scan and the corresponding oxidation peak at ~1.5 V on the reversible anodic scan are related to the Li⁺ intercalation–deintercalation processes (Yoon et al., 2014; Li B. et al., 2016; Pathak et al., 2018; Huang et al., 2020). Additionally, the reduction peak observed below 0.25 V can be associated with the conversion of W⁶⁺ to W⁰, which could cause the destruction of WO₃ lattice structure to a certain extent (Rastgoo–Deylami et al., 2021). The CV curves of the pure WO₃ bricks and WO₃ micro-spheres are also shown in **Figures 3B,C**, which exhibits similar shapes to that of hierarchical WO₃ agglomerates. For further comparison, **Figures 3D–F** illustrate the charge/discharge

curves of hierarchical WO₃ agglomerates, WO₃ bricks, and WO₃ micro-spheres under a stationary current density of 100 mA g⁻¹ within the voltage range of 0.01–3.0 V (vs. Li/Li⁺). Note that, from all the three electrodes, the difference in discharge-specific capacity is quite obvious between the first two cycles, but achieves stability in the subsequent cycles, which can be possibly explained by the stable surface state and electrochemical reversibility after the initial activation process (Liang et al., 2021a; Wang et al., 2021). However, the hierarchical WO₃ agglomerate electrode exhibits a higher discharge capacity of 487.6 mAh g⁻¹ after the first cycle, much better than WO₃ bricks (377.7 mAh g⁻¹) and WO₃ micro-spheres (393.6 mAh g⁻¹). The superior performance of the hierarchical WO₃ agglomerates was also observed in rate capability tests under various current densities, which is plotted in **Figure 3G**. A highly reversible capacity of 437.7 mAh g⁻¹ at 100 mA g⁻¹ is obtained, maintaining 121.4 mAh g⁻¹ when the current density reaches as high as 5,000 mA g⁻¹, demonstrating the best sustainable high current endurance of the hierarchical WO₃ agglomerates among all the samples. Regarding the long-term cycling stability (**Figure 3H**), reversible capacities of 522.7, 325.9, and 272.3 mAh g⁻¹ are retained for the hierarchical WO₃ agglomerate, WO₃ brick, and WO₃ micro-sphere electrodes, respectively, after 800 cycles at a high current density of 1,000 mA g⁻¹, indicating an outstanding long cycle life of the prepared hierarchical WO₃ agglomerates. We further compared the performance parameter with state-of-the-art representatively reported congeneric LIBs, which are shown in **Supplementary Figure S6** and **Supplementary Table S1**.

To study the dynamic characteristics of the hierarchical WO₃ agglomerate, WO₃ brick, and WO₃ micro-sphere electrodes, the EIS measurement was carried out (see **Figure 4A**). The depressed semicircle in high-frequency regions represents the charge transfer resistance at the interface of electrode/electrolyte, while the inclined line in low-frequency regions associated with the mass transfer process (Shaibani et al., 2020; Jiang et al., 2021). Obviously, the EIS result reveals that the hierarchical WO₃ agglomerate electrode shows significant smaller charge transfer resistance compared to that of WO₃ brick and WO₃ micro-sphere electrodes, which could be ascribed to the larger specific surface area and structural integrity of the hierarchical WO₃ agglomerate electrode. To seek an in-depth understanding of the electrode kinetics of the hierarchical WO₃ agglomerate electrode materials, the galvanostatic intermittent titration technique (GITT) is conducted to analyze the Li-ion diffusion coefficient (D_{Li^+}) during lithiation and delithiation. Of note, the cell was given five cycles at 100 mA g⁻¹ to reach its thermal equilibrium state (Chen et al., 2019). In addition, the batteries alternately discharged for 15 min, rested for 60 min, and then charged for 15 min in the same way. D_{Li^+} can be calculated *via*

$$D_{Li^+} = \frac{4}{\pi\tau} \left(\frac{mV_m}{MA} \right)^2 \left(\frac{\Delta E_s}{\Delta E_\tau} \right)^2 \quad (1)$$

where τ represents the relaxation time, and m , M , V_m , and A represent the active material mass, molar mass, molar volume,



and the electrode geometric area, respectively. ΔE_s denotes the voltage changes during the relaxation period, and ΔE_r is the variation during the current pulse. As shown in **Figure 4B**, the calculated D_{Li^+} of Li^+ is in the order of $10^{-11.5}$ – $10^{-13.1}$ $cm^2 s^{-1}$, which is highly comparable to those well-designed metal oxide-based electrode materials (Zhao et al., 2020). CV curves were also tested to explore the reaction kinetics of the hierarchical WO₃ agglomerate electrode. **Figure 4C** demonstrates the CV curves of the hierarchical WO₃ agglomerate electrode at various sweep rates from 0.2 to 5 $mV s^{-1}$ within a voltage range of 0.01–3 V. As the scan rates increase, the CV profiles remain similar except that the cathodic and anodic peaks slightly shift and gradually broaden. A power-law ($i = av^b$) can be used to describe the relationship between the peak current (i) and scan rate (v), where a and b are defined as adjustable parameters (He et al., 2014; Liu et al., 2021). In principle, a b value of 0.5 means that the current is controlled by semi-infinite diffusion, while 1.0 indicates a surface capacitive-controlled behavior (Wang et al., 2019; Fu et al., 2020). By fitting the profiles of $\log(i)$ as a function of $\log(v)$ (**Figure 4D**), the calculated b values of 0.71 and 0.51 are computed for the cathodic and anodic peaks, respectively, indicating that the charge storage of the hierarchical WO₃ agglomerates is mainly dominated by the joint effect of diffusion and capacitive-controlled processes (Hwang et al., 2019; Liang et al., 2021b).

To reveal the charge storage mechanism of the hierarchical WO₃ agglomerates, the *ex situ* XPS analyses are conducted at fully discharged/charged states to explore the valence state of tungsten

and oxygen elements. The high-resolution XPS of W 4f presented in **Figure 5A** shows that two peaks appeared at binding energies of 35.1 and 37.1 eV at the fully discharged state, which can be ascribed to the W 4f_{7/2} and W 4f_{5/2} of W⁶⁺, respectively (Tong et al., 2016). In addition, two other small W 4f core level peaks centered at 32.1 and 33.5 eV also emerge in the XPS spectra, indicative of the formation of elemental tungsten as a result of Li⁺ intercalation (Tong et al., 2016). After being fully charged (**Figure 5B**), the doublet at 34.9 and 37.1 eV are detected in the high-resolution XPS of W 4f, which corresponds to the W 4f_{7/2} and W 4f_{5/2} of W⁶⁺. **Figures 5C,D** show the O 1s XPS spectra of the hierarchical WO₃ agglomerates at fully discharged and charged stages. As demonstrated, the XPS measurement shows a stable typical peak located at 529.8 eV, which is attributed to the W-O bonding mode of WO₃ (Li P. et al., 2016), indicating that oxygen does not participate in charge compensation during cycling. According to previous works (Kumagai et al., 1996; Gu et al., 2007; Huang et al., 2008), the energy storage in WO₃ has been proved to be highly associated with lithium intercalation/de-intercalation during the cycling process. Combining with the XPS results, we further confirm that the charge storage mechanism of the prepared hierarchical WO₃ agglomerates firstly occurs with Li⁺ intercalation and then the conversion of partial tungsten elements during the discharging process, which can also be found in other metal oxides (Poizot et al., 2000; Grugeon et al., 2001).

Based on the above analysis and discussions, the reaction mechanism of the hierarchical WO₃ agglomerates in the charge/

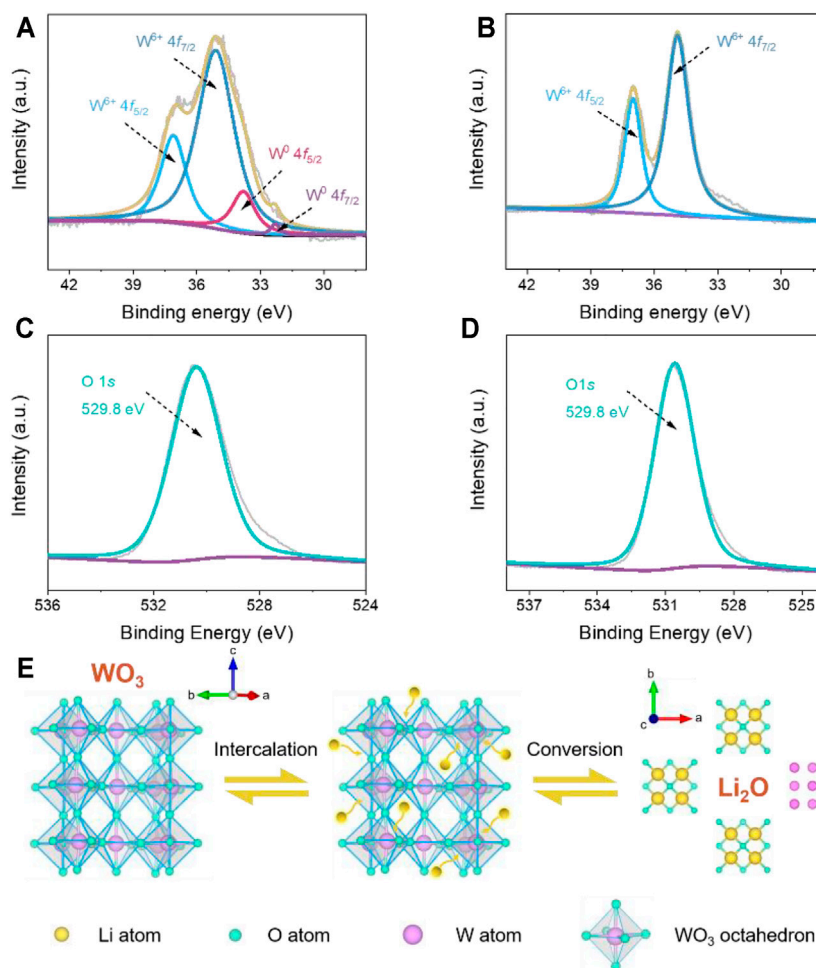
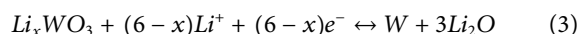
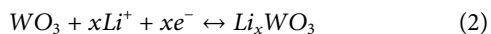


FIGURE 5 | (A, B) *Ex situ* XPS spectra of the W 4f region of fully discharged and charged hierarchical WO₃ agglomerate electrodes. **(C, D)** O 1s region of fully discharged and charged hierarchical WO₃ agglomerate electrodes. **(E)** Schematic illustration of the proposed charge storage mechanism for WO₃-based LIBs.

discharge processes can be schematically illustrated in **Figure 5E**, and the proposed mechanisms can be approximately expressed as follows (Wu and Yao, 2017; Wang et al., 2019):



The Li⁺ insertion and extraction reaction are represented by **Eq. 2**, and *x* represents the ratio of lithium ion to tungsten oxide. **Eq. 3** shows that the typical conversion reaction occurs at the electrode, where the zero-valent tungsten can be generated. The mechanistic insights into the energy storage processes in WO₃-based materials are helpful to design and prepare advanced electrode structures in enhancing the Li storage performances for high-energy LIBs.

CONCLUSION

To summarize, hierarchical WO₃ agglomerates assembled with straight and parallel aligned nanoribbons have been successfully

prepared by a facile hydrothermal approach, and introduced as a novel promising anode material for LIBs. The unique hierarchical agglomerate structure building by secondary 1D nanoribbons with a large interior space can effectively increase the electrode/electrolyte contact area, provide sufficient accessible active sites, and enable rapid transport of both Li ions and electrons. Electrochemical tests demonstrate that the prepared hierarchical WO₃ agglomerates show remarkable Li storage properties including high reversible specific capacity, outstanding rate capability, and excellent cycling stability, making it a very attractive anode for LIBs. This study paves the way to develop transition-metal-based electrode materials with well-designed architecture for applications in high-performance LIBs.

DATA AVAILABILITY STATEMENT

The original contributions presented in the study are included in the article/**Supplementary Material**. Further inquiries can be directed to the corresponding authors.

AUTHOR CONTRIBUTIONS

XD and YL contributed equally to this work. All authors listed have made a substantial, direct, and intellectual contribution to the work and approved it for publication.

FUNDING

HL acknowledges the support from the National Natural Science Foundation of China (51804173) and the Undergraduate

Innovation and Entrepreneurship Training Program. CZ acknowledges the support from Henan New Engineering Research and Practice Project (2020JGLX067).

SUPPLEMENTARY MATERIAL

The Supplementary Material for this article can be found online at: <https://www.frontiersin.org/articles/10.3389/fchem.2021.834418/full#supplementary-material>

REFERENCES

- Abakumov, A. M., Fedotov, S. S., Antipov, E. V., and Tarascon, J.-M. (2020). Solid State Chemistry for Developing Better Metal-Ion Batteries. *Nat. Commun.* 11 (1), 4976. doi:10.1038/s41467-020-18736-7
- Bekarevich, R., Pihosh, Y., Tanaka, Y., Nishikawa, K., Matsushita, Y., Hiroto, T., et al. (2020). Conversion Reaction in the Binder-free Anode for Fast-Charging Li-Ion Batteries Based on WO₃ Nanorods. *ACS Appl. Energ. Mater.* 3 (7), 6700–6708. doi:10.1021/acsaem.0c00844
- Chen, M., Hua, W., Xiao, J., Cortie, D., Chen, W., Wang, E., et al. (2019). NASICON-type Air-Stable and All-Climate Cathode for Sodium-Ion Batteries with Low Cost and High-Power Density. *Nat. Commun.* 10 (1), 1480. doi:10.1038/s41467-019-09170-5
- Dahbi, M., Yabuuchi, N., Fukunishi, M., Kubota, K., Chihara, K., Tokiwa, K., et al. (2016). Black Phosphorus as a High-Capacity, High-Capability Negative Electrode for Sodium-Ion Batteries: Investigation of the Electrode/Electrolyte Interface. *Chem. Mater.* 28 (6), 1625–1635. doi:10.1021/acs.chemmater.5b03524
- Di, J., Xu, H., Gai, X., Yang, R., and Zheng, H. (2019). One-step Solvothermal Synthesis of Feather Duster-like CNT@WO₃ as High-Performance Electrode for Supercapacitor. *Mater. Lett.* 246, 129–132. doi:10.1016/j.matlet.2019.03.070
- Du, Q.-k., Wu, Q.-x., Wang, H.-x., Meng, X.-j., Ji, Z.-k., Zhao, S., et al. (2021). Carbon Dot-Modified Silicon Nanoparticles for Lithium-Ion Batteries. *Int. J. Miner Metall. Mater.* 28 (10), 1603–1610. doi:10.1007/s12613-020-2247-1
- Duan, X., Xiao, S., Wang, L., Huang, H., Liu, Y., Li, Q., et al. (2015). Ionic Liquid-Modulated Preparation of Hexagonal Tungsten Trioxide Mesocrystals for Lithium-Ion Batteries. *Nanoscale* 7 (6), 2230–2234. doi:10.1039/C4NR05171A
- Eum, D., Kim, B., Kim, S. J., Park, H., Wu, J., Cho, S.-P., et al. (2020). Voltage Decay and Redox Asymmetry Mitigation by Reversible Cation Migration in Lithium-Rich Layered Oxide Electrodes. *Nat. Mater.* 19 (4), 419–427. doi:10.1038/s41563-019-0572-4
- Fu, Q., Zhu, X., Li, R., Liang, G., Luo, L., Chen, Y., et al. (2020). A Low-Strain V₃Nb₁₇O₅₀ Anode Compound for superior Li⁺ Storage. *Energ. Storage Mater.* 30, 401–411. doi:10.1016/j.ensm.2020.05.012
- Gao, Y., Rojas, T., Wang, K., Liu, S., Wang, D., Chen, T., et al. (2020). Low-temperature and High-Rate-Charging Lithium Metal Batteries Enabled by an Electrochemically Active Monolayer-Regulated Interface. *Nat. Energ.* 5 (7), 534–542. doi:10.1038/s41560-020-0640-7
- Grugeon, S., Laruelle, S., Herrera-Urbina, R., Dupont, L., Poizot, P., and Tarascon, J.-M. (2001). Particle Size Effects on the Electrochemical Performance of Copper Oxides toward Lithium. *J. Electrochem. Soc.* 148 (4), A285. doi:10.1149/1.1353566
- Gu, Z., Li, H., Zhai, T., Yang, W., Xia, Y., Ma, Y., et al. (2007). Large-scale Synthesis of Single-crystal Hexagonal Tungsten Trioxide Nanowires and Electrochemical Lithium Intercalation into the Nanocrystals. *J. Solid State. Chem.* 180 (1), 98–105. doi:10.1016/j.jssc.2006.09.020
- He, X., Wang, J., Kloepsch, R., Krueger, S., Jia, H., Liu, H., et al. (2014). Enhanced Electrochemical Performance in Lithium Ion Batteries of a Hollow Spherical Lithium-Rich Cathode Material Synthesized by a Molten Salt Method. *Nano Res.* 7 (1), 110–118. doi:10.1007/s12274-013-0378-7
- Hou, R., Li, H., Diao, M., Sun, Y., Liang, Y., Yu, Z., et al. (2022). Fast Electrochemical Activation of the Broadband Saturable Absorption of Tungsten Oxide Nanoporous Film. *Nano Res.* 15 (1), 326–332. doi:10.1007/s12274-021-3478-9
- Huang, K., Pan, Q., Yang, F., Ni, S., Wei, X., and He, D. (2008). Controllable Synthesis of Hexagonal WO₃ nanostructures and Their Application in Lithium Batteries. *J. Phys. D: Appl. Phys.* 41 (15), 155417. doi:10.1088/0022-3727/41/15/155417
- Huang, Y., Lu, R., Wang, M., Sakamoto, J., and Poudeu, P. F. P. (2020). Hexagonal-WO₃ Nanorods Encapsulated in Nitrogen and Sulfur Co-doped Reduced Graphene Oxide as a High-Performance Anode Material for Lithium Ion Batteries. *J. Solid State. Chem.* 282, 121068. doi:10.1016/j.jssc.2019.121068
- Hwang, C. H., Kim, H.-e., Nam, I., and Bang, J. H. (2019). Polygonal Multi-Polymorphed Li₄Ti₅O₁₂@rutile TiO₂ as Anodes in Lithium-Ion Batteries. *Nano Res.* 12 (4), 897–904. doi:10.1007/s12274-019-2320-0
- Jiang, Q., Zhang, W.-q., Zhao, J.-c., Rao, P.-h., and Mao, J.-f. (2021). Superior Sodium and Lithium Storage in Strongly Coupled Amorphous Sb₂S₃ Spheres and Carbon Nanotubes. *Int. J. Miner Metall. Mater.* 28 (7), 1194–1203. doi:10.1007/s12613-021-2259-5
- Kumagai, N., Kumagai, N., Umetzu, Y., Tanno, K., and Pereira-Ramos, J. P. (1996). Synthesis of Hexagonal Form of Tungsten Trioxide and Electrochemical Lithium Insertion into the Trioxide. *Solid State Ionics* 86-88, 1443–1449. doi:10.1016/0167-2738(96)00327-X
- Lee, S.-K., Kim, H., Bang, S., Myung, S.-T., and Sun, Y.-K. (2021). WO₃ Nanowire/Carbon Nanotube Interlayer as a Chemical Adsorption Mediator for High-Performance Lithium-Sulfur Batteries. *Molecules* 26 (2), 377. doi:10.3390/molecules26020377
- Li, B., Li, X., Li, W., Wang, Y., Uchaker, E., Pei, Y., et al. (2016a). Mesoporous Tungsten Trioxide Polyaniline Nanocomposite as an Anode Material for High-Performance Lithium-Ion Batteries. *ChemNanoMat* 2 (4), 281–289. doi:10.1002/cnma.201500208
- Li, H., Hu, Z., Xia, Q., Zhang, H., Li, Z., Wang, H., et al. (2021a). Operando Magnetometry Probing the Charge Storage Mechanism of CoO Lithium-Ion Batteries. *Adv. Mater.* 33 (12), 2006629. doi:10.1002/adma.202006629
- Li, H., Zhang, X., Zhao, Z., Hu, Z., Liu, X., and Yu, G. (2020). Flexible Sodium-Ion Based Energy Storage Devices: Recent Progress and Challenges. *Energ. Storage Mater.* 26, 83–104. doi:10.1016/j.ensm.2019.12.037
- Li, P., Li, X., Zhao, Z., Wang, M., Fox, T., Zhang, Q., et al. (2016b). Correlations Among Structure, Composition and Electrochemical Performances of WO₃ Anode Materials for Lithium Ion Batteries. *Electrochimica Acta* 192, 148–157. doi:10.1016/j.electacta.2016.01.199
- Li, Q., Li, H., Xia, Q., Hu, Z., Zhu, Y., Yan, S., et al. (2021b). Extra Storage Capacity in Transition Metal Oxide Lithium-Ion Batteries Revealed by *In Situ* Magnetometry. *Nat. Mater.* 20, 76–83. doi:10.1038/s41563-020-0756-y
- Li, Y., Chang, K., Tang, H., Li, B., Qin, Y., Hou, Y., et al. (2019). Preparation of Oxygen-Deficient WO₃-Nanosheets and Their Characterization as Anode Materials for High-Performance Li-Ion Batteries. *Electrochimica Acta* 298, 640–649. doi:10.1016/j.electacta.2018.12.137
- Liang, H., Hu, Z., Zhao, Z., Chen, D., Zhang, H., Wang, H., et al. (2021a). Dendrite-structured FeF₂ Consisting of Closely Linked Nanoparticles as Cathode for High-Performance Lithium-Ion Capacitors. *J. Energ. Chem.* 55, 517–523. doi:10.1016/j.jechem.2020.07.031
- Liang, H., Zhang, H., Zhao, L., Chen, Z., Huang, C., Zhang, C., et al. (2022). Layered Fe₂(MoO₄)₃ Assemblies with Pseudocapacitive Properties as Advanced Materials for High-Performance Sodium-Ion Capacitors. *Chem. Eng. J.* 427, 131481. doi:10.1016/j.cej.2021.131481

- Liang, H., Zhang, Y., Hao, S., Cao, L., Li, Y., Li, Q., et al. (2021b). Fast Potassium Storage in Porous CoV₂O₆ Nanosphere@graphene Oxide towards High-Performance Potassium-Ion Capacitors. *Energ. Storage Mater.* 40, 250–258. doi:10.1016/j.ensm.2021.05.013
- Liu, C., Wang, C., Meng, X., Li, X., Qing, Q., Wang, X., et al. (2020a). Tungsten Nitride Nanoparticles Anchored on Porous Borocarbonitride as High-Rate Anode for Lithium Ion Batteries. *Chem. Eng. J.* 399, 125705. doi:10.1016/j.cej.2020.125705
- Liu, L., Zhao, Z., Hu, Z., Lu, X., Zhang, S., Huang, L., et al. (2020b). Designing Uniformly Layered FeTiO₃ Assemblies Consisting of Fine Nanoparticles Enabling High-Performance Quasi-Solid-State Sodium-Ion Capacitors. *Front. Chem.* 8, 371. doi:10.3389/fchem.2020.00371
- Liu, Z., Luo, X., Qin, L., Fang, G., and Liang, S. (2021). Progress and prospect of Low-Temperature Zinc Metal Batteries. *Adv. Powder Mater.* doi:10.1016/j.apmate.2021.10.002
- Luo, Y., Wang, C., and Wang, X. (2021). Fast Energy Storage Performance of CoFe₂O₄/CNTs Hybrid Aerogels for Potassium Ion Battery. *J. Colloid Interf. Sci.* 600, 820–827. doi:10.1016/j.jcis.2021.05.088
- Pachfule, P., Shinde, D., Majumder, M., and Xu, Q. (2016). Fabrication of Carbon Nanorods and Graphene Nanoribbons from a Metal-Organic Framework. *Nat. Chem* 8 (7), 718–724. doi:10.1038/nchem.2515
- Pathak, R., Gurung, A., Elbohy, H., Chen, K., Reza, K. M., Bahrami, B., et al. (2018). Self-recovery in Li-Metal Hybrid Lithium-Ion Batteries via WO₃ Reduction. *Nanoscale* 10 (34), 15956–15966. doi:10.1039/c8nr01507d
- Poizat, P., Laruelle, S., Grugnon, S., Dupont, L., and Tarascon, J.-M. (2000). Nano-sized Transition-Metal Oxides as Negative-Electrode Materials for Lithium-Ion Batteries. *Nature* 407 (6803), 496–499. doi:10.1038/35035045
- Qu, G., Wang, J., Liu, G., Tian, B., Su, C., Chen, Z., et al. (2019). Vanadium Doping Enhanced Electrochemical Performance of Molybdenum Oxide in Lithium-Ion Batteries. *Adv. Funct. Mater.* 29 (2), 1805227. doi:10.1002/adfm.201805227
- Rastgoo-Deylami, M., Javanbakht, M., Omidvar, H., Hooshyari, K., Salarizadeh, P., and Askari, M. B. (2021). Nickel-doped Monoclinic WO₃ as High Performance Anode Material for Rechargeable Lithium Ion Battery. *J. Electroanalytical Chem.* 894, 115383. doi:10.1016/j.jelechem.2021.115383
- Sasidharan, M., Gunawardhana, N., Yoshio, M., and Nakashima, K. (2012). WO₃ Hollow Nanospheres for High-Lithium Storage Capacity and Good Cyclability. *Nano Energy* 1 (3), 503–508. doi:10.1016/j.nanoen.2012.03.003
- Shaibani, M., Mirshekarloo, M. S., Singh, R., Easton, C. D., Cooray, M. C. D., Eshraghi, N., et al. (2020). Expansion-tolerant Architectures for Stable Cycling of Ultrahigh-Loading Sulfur Cathodes in Lithium-Sulfur Batteries. *Sci. Adv.* 6 (1), eaay2757. doi:10.1126/sciadv.aay2757
- Tong, H., Xu, Y., Cheng, X., Zhang, X., Gao, S., Zhao, H., et al. (2016). One-pot Solvothermal Synthesis of Hierarchical WO₃ Hollow Microspheres with superior Lithium Ion Battery Anode Performance. *Electrochimica Acta* 210, 147–154. doi:10.1016/j.electacta.2016.05.154
- Tu, J., Lei, H., Yu, Z., and Jiao, S. (2018). Ordered WO_{3-x} Nanorods: Facile Synthesis and Their Electrochemical Properties for Aluminum-Ion Batteries. *Chem. Commun.* 54 (11), 1343–1346. doi:10.1039/C7CC09376D
- Wang, H., Jiang, Y., and Manthiram, A. (2018). Long Cycle Life, Low Self-Discharge Sodium-Selenium Batteries with High Selenium Loading and Suppressed Polyselenide Shuttling. *Adv. Energ. Mater.* 8 (7), 1701953. doi:10.1002/aenm.201701953
- Wang, H., Zhao, L., Zhang, H., Liu, Y., Yang, L., Li, F., et al. (2021). Revealing the Multiple Cathodic and Anodic Involved Charge Storage Mechanism in an FeSe₂ Cathode for Aluminum-Ion Batteries by *In Situ* Magnetometry. *Energy Environ. Sci.* 15, 311–319. doi:10.1039/D1EE03070A
- Wang, L., Huang, K.-W., Chen, J., and Zheng, J. (2019). Ultralong Cycle Stability of Aqueous Zinc-Ion Batteries with Zinc Vanadium Oxide Cathodes. *Sci. Adv.* 5 (10), eaax4279. doi:10.1126/sciadv.aax4279
- Wu, X., and Yao, S. (2017). Flexible Electrode Materials Based on WO₃ Nanotube Bundles for High Performance Energy Storage Devices. *Nano Energy* 42, 143–150. doi:10.1016/j.nanoen.2017.10.058
- Xiao, Y., Jiang, M., and Cao, M. (2021a). Developing WO₃ as High-Performance Anode Material for Lithium-Ion Batteries. *Mater. Lett.* 285, 129129. doi:10.1016/j.matlet.2020.129129
- Xiao, Z., Yu, Z., Ma, X., and Xu, C. (2021b). S, N-Codoped Carbon Capsules with Microsized Entrance: Highly Stable S Reservoir for Li-S Batteries. *Adv. Powder Technol.* 32 (5), 1757–1765. doi:10.1016/j.apt.2021.03.031
- Yao, S., Qu, F., Wang, G., and Wu, X. (2017). Facile Hydrothermal Synthesis of WO₃ Nanorods for Photocatalysts and Supercapacitors. *J. Alloys Compd.* 724, 695–702. doi:10.1016/j.jallcom.2017.07.123
- Yao, Y., Chen, M., Xu, R., Zeng, S., Yang, H., Ye, S., et al. (2018). CNT Interwoven Nitrogen and Oxygen Dual-Doped Porous Carbon Nanosheets as Free-Standing Electrodes for High-Performance Na-Se and K-Se Flexible Batteries. *Adv. Mater.* 30 (49), 1805234. doi:10.1002/adma.201805234
- Yoon, S., Woo, S.-G., Jung, K.-N., and Song, H. (2014). Conductive Surface Modification of Cauliflower-like WO₃ and its Electrochemical Properties for Lithium-Ion Batteries. *J. Alloys Compd.* 613, 187–192. doi:10.1016/j.jallcom.2014.06.010
- Yu, M., Sun, H., Sun, X., Lu, F., Hu, T., Wang, G., et al. (2013). 3D WO₃ Nanowires/graphene Nanocomposite with Improved Reversible Capacity and Cyclic Stability for Lithium Ion Batteries. *Mater. Lett.* 108, 29–32. doi:10.1016/j.matlet.2013.06.067
- Yue, L., Ma, C., Yan, S., Wu, Z., Zhao, W., Liu, Q., et al. (2022). Improving the Intrinsic Electronic Conductivity of NiMoO₂ Anodes by Phosphorous Doping for High Lithium Storage. *Nano Res.* 15 (1), 186–194. doi:10.1007/s12274-021-3455-3
- Zhang, F., and Qi, L. (2016). Recent Progress in Self-Supported Metal Oxide Nanoarray Electrodes for Advanced Lithium-Ion Batteries. *Adv. Sci.* 3 (9), 1600049. doi:10.1002/advs.201600049
- Zhao, Z., Hu, Z., Jiao, R., Tang, Z., Dong, P., Li, Y., et al. (2019). Tailoring Multi-Layer Architected FeS₂@C Hybrids for superior Sodium-, Potassium- and Aluminum-Ion Storage. *Energ. Storage Mater.* 22, 228–234. doi:10.1016/j.ensm.2019.01.022
- Zhao, Z., Hu, Z., Li, Q., Li, H., Zhang, X., Zhuang, Y., et al. (2020). Designing Two-Dimensional WS₂ Layered Cathode for High-Performance Aluminum-Ion Batteries: From Micro-assemblies to Insertion Mechanism. *Nano Today* 32, 100870. doi:10.1016/j.nantod.2020.100870

Conflict of Interest: The authors declare that the research was conducted in the absence of any commercial or financial relationships that could be construed as a potential conflict of interest.

Publisher's Note: All claims expressed in this article are solely those of the authors and do not necessarily represent those of their affiliated organizations, or those of the publisher, the editors, and the reviewers. Any product that may be evaluated in this article, or claim that may be made by its manufacturer, is not guaranteed or endorsed by the publisher.

Copyright © 2022 Dong, Liu, Zhu, Ou, Zhang, Lan, Guo, Zhang, Liu, Ju, Miao, Zhang and Li. This is an open-access article distributed under the terms of the Creative Commons Attribution License (CC BY). The use, distribution or reproduction in other forums is permitted, provided the original author(s) and the copyright owner(s) are credited and that the original publication in this journal is cited, in accordance with accepted academic practice. No use, distribution or reproduction is permitted which does not comply with these terms.